Electronic structure of metallic liquid Se-Te alloys

Shaw Shya Kao and Melvin Cutler
Physics Department, Oregon State University, Corvallis, Oregon 97331
(Received 13 October 1987)

Experimental data for the electrical conductivity σ, the thermopower S, and the magnetic susceptibility χ are analyzed for alloys Se_xTe_{100-x} in the metallic and near-metallic range of compositions $x=0$ to 50. Comparison of the behavior of σ and S in the region where the metallic approximation to the transport coefficients is valid shows that $\sigma(E_F)$ is proportional to the Fermi energy E_F for $x=10$ and 20. In view of the validity of the diffusive model for transport, this corresponds to a parabolic density of states $N(E_F)$. At $x=30$, it is found that $N(E_F)$ changes to a linear dependence on E_F, in keeping with the beginning of band tailing as the Fermi energy approaches the edge of the valence band. For $x \leq 30$, the experimental behavior of the paramagnetic susceptibility χ_P confirms independently the shape of $N(E_F)$ deduced from σ and S, and comparison of the three experimental variables yields numerical values for the band parameters. At $x=40$ and 50, where analysis requires the use of Fermi-Dirac integrals, the behavior of σ and S is still consistent with a linear $N(E)$, but the behavior of the experimental χ_P indicates that the spin states are separating from the valence band as the temperature is decreased.

I. INTRODUCTION

Selenium and tellurium are group-VI elements which form a homogeneous liquid alloy over all compositions Se_xTe_{100-x}. This alloy system has attracted considerable interest because it has a continuous electronic change from a high-resistivity semiconductor at low temperature T and at high selenium concentrations, to a poorly conducting metal at high T or at high tellurium concentrations.[1,2] The transition to metallic behavior is shown by studies of the electrical conductivity σ, thermopower S, and the magnetic susceptibility χ.[3,4] This electronic transition to a metal seems to be correlated to a thermodynamic transition, as indicated by an anomalous increase in density,[5] and maxima in the compressibility[6] and the heat capacity[7] as T is increased. Many authors believe that there is also a correlation to an increase in the coordination number, but this is less clearly supported by experimental evidence.

The purpose of this paper is to make a detailed examination of the electronic behavior in the metallic and near-metallic range, with the goal of learning as much as possible about the electronic structure and how it is affected by temperature and composition. In earlier work by Gardner and Cutler,[8] a correlation in the behavior of σ and χ was found which shows that σ is proportional to the square of the density of states at the Fermi energy $N(E_F)$, as expected for the diffusive mechanism of electronic transport in highly disordered materials. In the present work, we find it possible to use a method, previously used in Tl-Te alloys, to determine the shape of $N(E_F)$ from the dependence of S on σ.[2] We also analyze the joint behavior of S, σ, and χ to test the theoretical model for consistency, to deduce information about the behavior of E_F and related quantities as T and x are changed, and to determine the parameters describing the electronic structure. Finally, a comparison of the calculated band susceptibility with the experimental values at compositions near the metal-semiconductor transition is made, which shows clear evidence of a separation from the valence band of states which are responsible for the paramagnetic susceptibility.

II. BASIS OF THE ANALYSIS

A. Experimental data

For the most part, the analysis is based on new measurements of S and σ which we made recently in the composition range 0–50 at. % Se using methods described previously.[9] The experimental curves are shown in Figs. 1 and 2. These results agree reasonably well with those reported previously by Perron[1] and others.[10] For the magnetic susceptibility, we have used data reported previously by Gardner and Cutler.[8]

B. Theoretical equations

The description of the electronic structure of highly disordered materials such as liquid semiconductors centers on the density of states $N(E)$. The positive thermopower indicates that the Fermi energy E_F is in the valence band. For mathematical convenience we express $N(E)$ as a quantity proportional to a power of the energy E of a hole, i.e., it is measured downwards in a scale of electron energies, as indicated in Fig. 3. Thus,

$$N(E)=BE^b , \tag{1}$$

where B and b are constants.

In keeping with experimental results,[8] the behavior of

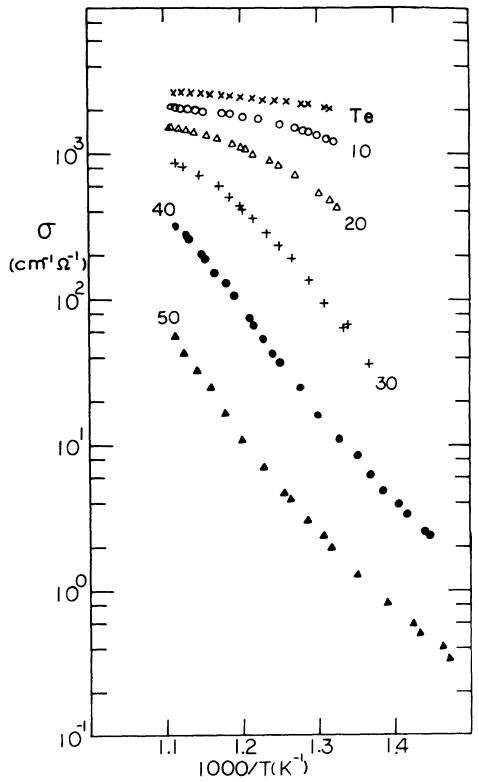

FIG. 1. Electrical conductivity vs T for 0–50 at. % Se.

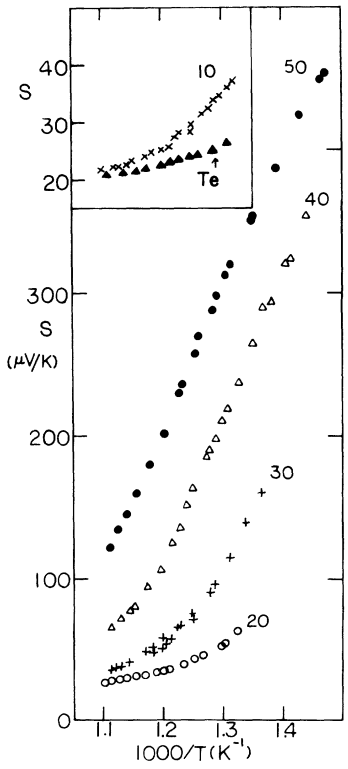

FIG. 2. Thermopower vs T for 0–50 at. % Se. The results for $x=0$ and 10 are given in the inset, with a different scale for S.

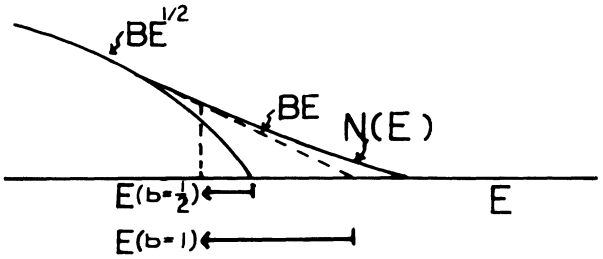

FIG. 3. Diagram for the electronic structure, showing the approximation of the band tail by superposition of linear and parabolic curves for $N(E)$.

the conductivity $\sigma(E)$ of states at energy E is described by the diffusive equation:

$$\sigma(E)=A\,[N(E)]^2\,, \tag{2}$$

where A is a constant.[11] The transport coefficients σ and S are determined by

$$\sigma=-\int\sigma(E)\frac{\delta f}{\delta E}dE \tag{3}$$

and

$$S=\frac{k}{e}\int\frac{(E-E_F)}{kT}\frac{\sigma(E)\frac{\delta f}{\delta E}}{\sigma}\,, \tag{4}$$

where $f(E)$ is the Fermi-Dirac probability that a hole is at energy E.

In most of the analysis, we use the metallic approximation, which is accurate when the Fermi energy for holes $E_F \gg kT$. On substituting Eqs. (1) and (2), this yields

$$\sigma=AB^2E_F^{2b} \tag{5}$$

and

$$S=(\pi^2k^2T/3e)[d\ln\sigma/dE]_{E_F}\,. \tag{6}$$

The Pauli susceptibility is related to the density of states $N(E)$ by

$$\chi_P=\mu_B^2\int f(E)(dN/dE)dE\,, \tag{7}$$

where μ_B is the Bohr magnetron. With the metallic approximation this yields

$$\chi_P=(\alpha-\beta)\mu_B^2N(E_F)\,, \tag{8}$$

where correction parameters have been added for the uncertain effects of the diamagnetic susceptibility (β) and correlation (α). In a free-electron gas, $\alpha-\beta=\frac{2}{3}$.

III. THE SHAPE OF $N(E_F)$

In the metallic range, according to Eq. (6), S is proportional to the derivative of σ with respect to E_F. This equation can be integrated, using Eq. (5) to express the dependence of E_F on σ, to obtain a relation between S and σ in the form

$$\ln(S/T)=\ln(2b\pi^2kAB^2/3e)-(1/2b)\ln\sigma \ . \quad (9)$$

In accordance with this equation, plots were made of $\ln(S/T)$ versus $\ln\sigma$ for compositions $x=10$–40, which are shown in Fig. 4. It is seen that the curves have nearly constant slopes which decrease with increasing x. The slope for $x\leq 20$ corresponds to $b=0.52$. This agrees well with the value $b=\frac{1}{2}$ expected for the conventional parabolic shape of $N(E)$.

The decreasing slope for larger x may be caused either by a changing shape for $N(E_F)$ or by inaccuracy of the metallic approximation when E_F gets too small. To check on the latter possibility, more accurate expressions were used in place of Eq. (9), which are based on Fermi-Dirac integrals discussed in Sec. V. On doing this, we found little change from the metallic approximation. The slope corresponds fairly well with the value $b=1$, which indicates that the curvature of $N(E_F)$ is decreasing with decreasing E_F. This is consistent with the development of band tailing at energies near the band edge, as expected for a highly disordered system. This is illustrated in Fig. 3. For $x=40$, we find that the metallic approximation is inaccurate. It is necessary to use expressions involving Fermi-Dirac integrals, as described in Sec. V.

IV. DEPENDENCE OF BAND PARAMETERS ON COMPOSITION

In this section we examine the extent to which the electronic behavior is consistent with the existence of a rigid-valence-band density of states $N(E)$, in which changes in the electronic properties with T and x are due solely to changes in E_F. In doing this, it has been convenient to replace E_F by the hole density n as the changing parameter, where

$$n=\int f(E)N(E)dE \ . \quad (10)$$

In the metallic approximation we get from Eq. (1)

$$n=BE_F^{b+1}/(b+1) \ , \quad (11)$$

assuming, of course, that $N(E)$ has the same shape over the whole range of E_F under consideration.

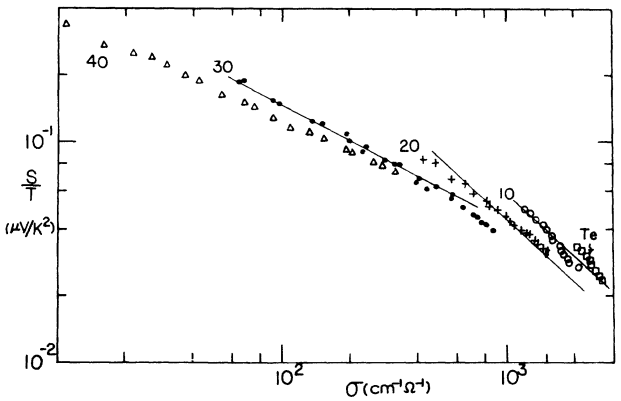

FIG. 4. Plots of $\ln(S/T)$ vs $\ln\sigma$ for $x=0$, 10, 20, 30, and 40.

σ, S, and χ_P can each be expressed in terms of E_F with the use of Eqs. (1), (5), (6), and (8). On inverting these expressions, and using Eq. (11) to replace E_F with n, expressions for N in terms of the three different experimental parameters are obtained:

$$n_\chi=[B/(1+b)][\chi_P/(\alpha-\beta)B]^{(1+b)/b} \ , \quad (12)$$

$$n_\sigma=[B/(1+b)](\sigma/AB^2)^{(1+b)/2b} \ , \quad (13)$$

$$n_S=[B/(1+b)](2b\pi^2k^2T/3eS)^{1+b} \ . \quad (14)$$

According to Eqs. (12)–(14), n is proportional to χ_P^3, $\sigma^{1.5}$, and $(T/S)^{1.5}$, so that plots of these functions on a logarithmic scale versus T should give parallel curves for a given composition. If the curves are parallel, one can obtain the ratios of the constants of proportionality from the shifts necessary to superpose the curves. In Fig. 5, we show plots of $\log_{10}n_\chi$, $\log_{10}n_\sigma$, and $\log_{10}n_S$, calculated with $b=0.5$ for $x=10$, 20, and 30. For each composition, the curves are shifted vertically so that they superpose, or else to show clearly the deviations from a consistent shape.

It is seen that the three curves superpose reasonably well for $x=20$. The magnitudes of the two shifts to superpose the three curves provide quantitative information about the parameters for this composition. There are three of them in Eqs. (12)–(14): A, B, and $\alpha-\beta$. Two of them can be calculated if the third is known. The range

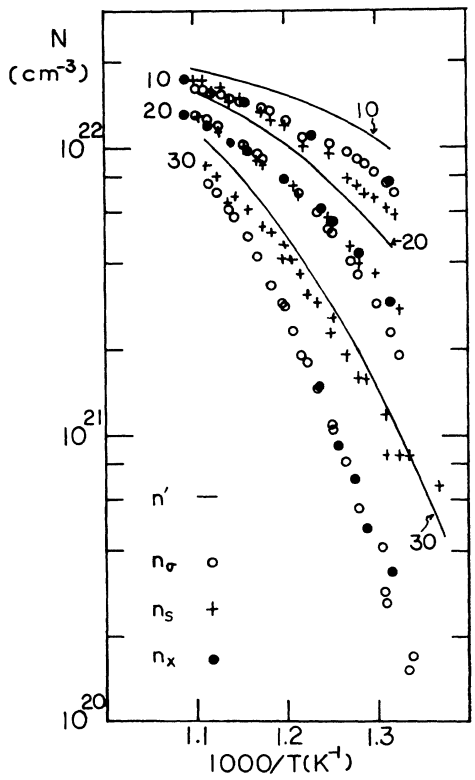

FIG. 5. Plots of n_x, n_s, and n_σ vs T^{-1} for $x=10$, 20, and 30 assuming $b=0.5$. The solid curves for n' are results corrected to include contributions from the band tail.

TABLE I. Valence-band parameters.

x (at. % Se)	A ($10^3\ \Omega^{-1}\ cm^{-1}\ atom^2\ eV^2$)	B ($atom^{-1}\ eV^{-1-b}$)	AB^2 ($10^3\ \Omega^{-1}\ cm^{-1}\ eV^{-2b}$)	b	T_t (K)
10	2.49	0.92	2.13	0.5	
20	1.97	0.96	1.83	0.5	753
30	1.52	1.00	1.50	0.5	838
	1.54	0.73	0.82	1.0	
40	>1.35	<0.78	0.449	1.0	898
50	>0.74	<0.78	0.259	1.0	983

of possible values of $\alpha-\beta$ seems most restricted, and one might expect it to be least likely to change with composition. Therefore we have calculated A and B assuming that $\alpha-\beta=1$. The values are listed in Table I.

For $x=10$, n_σ and n_χ superpose well, but n_S has an appreciable discrepancy. This seems to be due to experimental error, since a curve based on the thermopower data by Perron[1] fits well. The change in our S values necessary to give a good fit is not very large—less than 5 μV/K. The corresponding values of A and B, listed in Table I, show agreement in the value of B for $x=20$, and a somewhat larger value for A.

It is seen in Fig. 5 that the curves for $x=30$ have different slopes. This is not surprising, since the plot in Fig. 4 indicates that b is equal to 1.0 rather than 0.5. In Fig. 6, we show the three curves calculated from χ_P^2, σ^1, and $(T/S)^2$, corresponding to $b=1$, and it is seen that they match very well. The values of A and B are given in Table I. The value of A continues to decrease with x. The value of B is not to be compared with the previous ones because of the change in b.

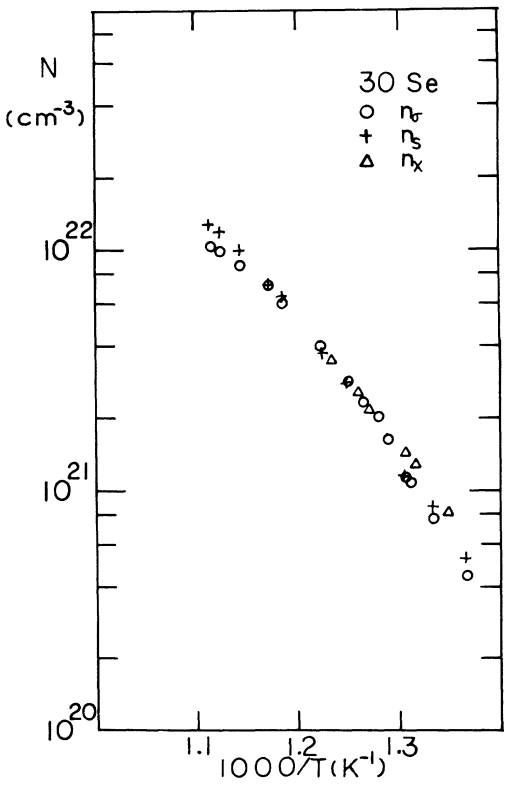

FIG. 6. Plots of n_x, n_s, and n_σ vs T^{-1} for $x=30$ assuming $b=1.0$.

The magnitudes of n in Figs. 5 and 6 correspond to the calculations based on $\alpha-\beta=1$. It is to be noted that n is smaller for $x=20$ than for $x=30$, indicating apparently that there are fewer empty states in the band for the more metallic composition. This reflects the fact that the fit of the data to a parabolic band model for $x\leq 20$ ignores the extra states near the top of the valence band due to the band tailing, and indicated by the sketch in Fig. 3. We shall show in Sec. V that it is possible to patch together these two representations of $N(E_F)$ to get a smooth change in n with x and T.

V. THE TRANSITION REGION

For $x=40$ and 50, neither the metallic approximation nor the Maxwell-Boltzmann approximation provides accurate solutions to Eqs. (3), (4), and (7), and it is necessary to use Fermi-Dirac integrals in the analysis.[12] In doing this, it is necessary to choose in advance the exponent b in the density-of-states expression [Eq. (1)]. The validity of the chosen value can be tested by trying to superpose a theoretically derived curve on an experimental plot of $\log_{10}(\sigma/T^{2b})$ versus S. It was found that good fits could be obtained only with $b=1$, as shown in Fig. 7.

For this value of b, the expressions derived from Eqs. (3) and (4) are

$$\sigma=2AB^2(kT)^2F_1(\xi) \tag{15}$$

and

$$S=(k/e)\{[3F_2(\xi)/2F_1(\xi)]-\xi\}\ , \tag{16}$$

where $\xi=E_F/kT$ and $F_n(\xi)$ is the integral

$$F_n(\xi)=\int_0^\infty x^n[1+\exp(x-\xi)]^{-1}dx\ . \tag{17}$$

The theoretical curve relating σ/T^2 to S in Fig. 7 is obtained by eliminating ξ in Eqs. (15) and (16). In this case, the magnitude of the shift which superposes itself on the experimental curves yields the values of AB^2, which are listed in Table I.

A similar comparison with experiment can be made for the paramagnetic susceptibility. No agreement could be found for any value of b. The theoretical expression for χ_P for $b=1$ derived from Eq. (7) is

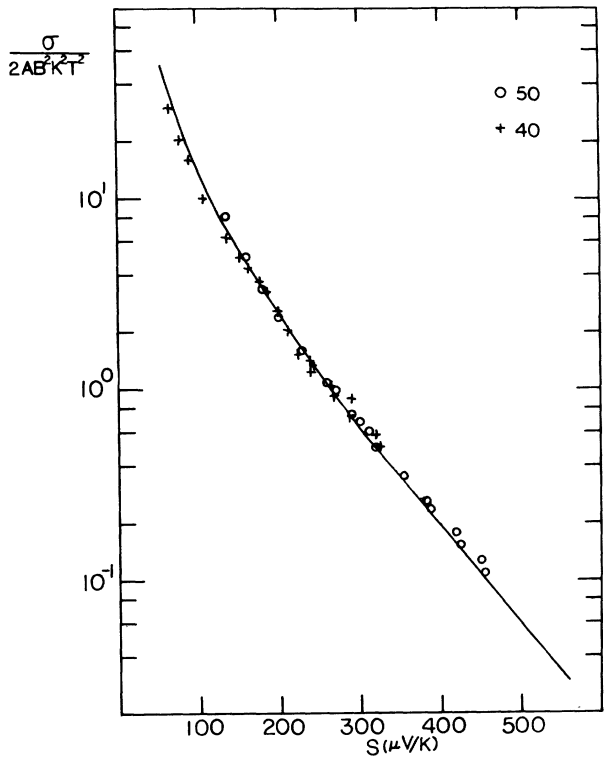

FIG. 7. Comparison of theoretical and experimental plots of σ/T^2 vs S for $x=40$ and 50. The experimental values of AB^2 are given in Table I.

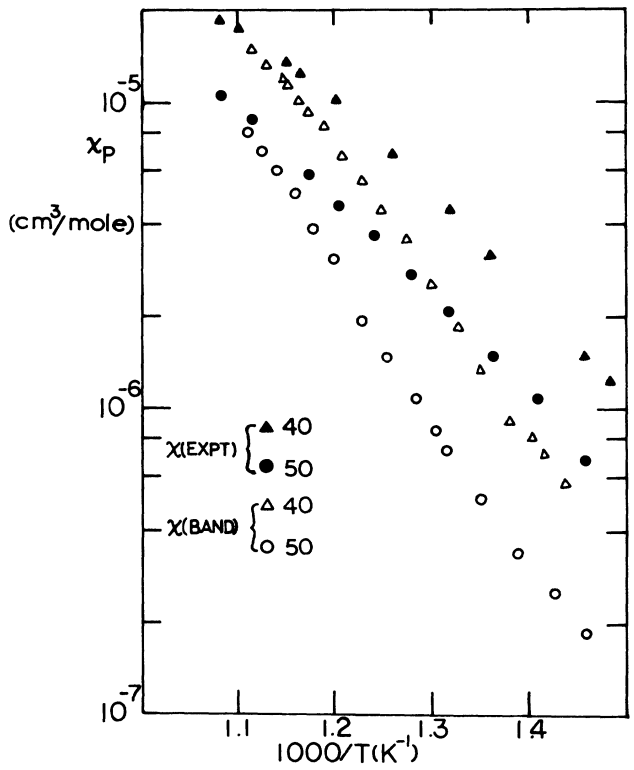

FIG. 8. Comparison of experimental χ_P vs T^{-1} with theory. The theoretical curves are drawn with values of B chosen to match points at the highest T.

$$\chi_P=\mu_B^2 BkTF_0(\xi)\ . \tag{18}$$

Experimental data for $S(T)$ together with Eq. (16) yields $\xi(T)$, and Eq. (18) can then be used to calculate the band contribution to χ_P within a constant factor corresponding to the unknown value of B. The theoretical χ_P curves for $x=40$ and 50 are compared with the experimental curves in Fig. 8, using values of B which match the points at the highest temperature (these values of B, which are listed in Table I, are maximum values consistent with available data, and the corresponding values of A in the table are minimum values). It is seen that the experimental curve drops much more slowly with decreasing temperature than the theoretical curves. The results in Fig. 7 show that the theory for band behavior adequately describes σ and S. So our conclusion is that part of the observed paramagnetism in this region of composition and temperature is due to states outside of the valence band. The shift of the paramagnetism to states external to the valence band is consistent with merging of states of an acceptor band with the valence band as x or T is increased. This mechanism was proposed some time ago by one of us to explain the metal transition in this alloy system.[2]

To what extent can the inferred values of $N(E_F)$ at the different compositions be placed on a common curve, as required by a rigid band model? The shape changes from parabolic at $x\leq 20$ to linear at $x=30$. When common values of $N(E_F)$ for these two compositions are superposed, as shown in Fig. 9, it requires a shift in the zero in E_F for the parabolic band to 0.42 eV in the linear band. The points merge smoothly to form a common curve. The curve for $x=10$ is also shown. It is somewhat lower, reflecting the slightly smaller value of B. This small discrepancy seems to be within the accuracy to be expected of our analysis.

In Fig. 10 we show the dependence of E_F in our synthesized rigid band on x and T. For $x\leq 20$, the zero of the Fermi energy has been shifted to 0.42 eV. The large

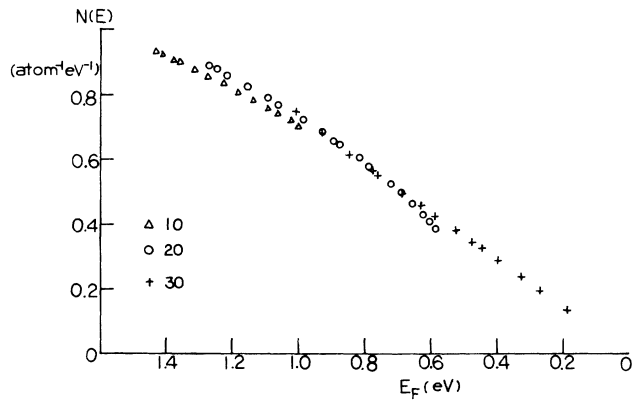

FIG. 9. Composite density-of-states curves obtained by setting $E_F=0$ for the parabolic bands to $E_F=0.42$ eV in the linear band.

slopes in $x=40$ and 50 at high temperatures are believed to be the effect of the absorption of the acceptor band states into the valence band. This rapid decrease of E_F with T is the cause of the rapid rise in the conductivity, with an apparent activation energy of 1.3 eV.

The effects of this phenomenon can be seen more clearly in the plots of the calculated acceptor band spin density for $x=40$ and 50 shown in Fig. 11. This was calculated by subtracting the valence-band contribution to χ_P shown in Fig. 8 from the experimental value, and using the Curie law to deduce the acceptor band spin density.[13] At low T, the acceptor band spin density has an Arrhenius-law behavior that is observed in Se-rich alloys. But at about 800 K, it goes through a maximum and decreases at higher T as the result, in our interpretation, of absorption of the acceptor band into the valence band.

Using the composite density-of-states curve in Fig. 9 together with the Fermi energy data in Fig. 10, we have constructed curves for the hole density as a function of temperature shown in Fig. 5 for $x=10$, 20, and 30. They show a continuously decreasing activation energy as x is decreased and T is increased. The largest values, at low T for $x=30$, exceed the activation energy 0.6–0.7 eV observed for the paramagnetic centers in the Se-rich alloys, which presumably represents the energy of formation of dangling bonds. The reason seems likely to be that it reflects the process of merging the acceptor band with the valence band. The fact that the slope continues to decrease after the band merging is complete, to activation energies <0.6 eV, may be due to chemical saturation. In this region, the spin density is approaching the concentration of atoms ($\approx 2.7\times 10^{22}$ cm^{-3}).

VI. CONCLUSIONS

In summary, relatively straightforward analysis in terms of the metallic approximation for σ, S, and χ_P in the composition range $x \leq 30$ shows that the experimental behavior of these parameters is consistent with diffusive transport in a valence band whose density of states has a parabolic shape for $x \leq 20$ and is linear in energy for $x=30$. In this region, the dependence of the valence-band hole density n on x and T inferred from σ and S is consistent with the behavior of χ_P. Approximate values of the theoretical parameters describing the shape of $N(E)$ and the diffusive transport are calculated subject to an assumption about the value of the magnetic susceptibility parameter $\alpha-\beta$. As x increases and T decreases, E_F moves toward the band edge. For $x=40$ and 50, the metallic approximation is inadequate, and theoretical relations involving Fermi-Dirac integrals must be used. It is found that σ and S continue to follow the theoretical relations indicated for a linear density-of-states curve. But the values of χ_P expected for the holes in the band fall below the experimental curve as T is decreased. This discrepancy is interpreted to be the result of the separation from the valence band of states which form the acceptor band in the semiconductor range of x and T.

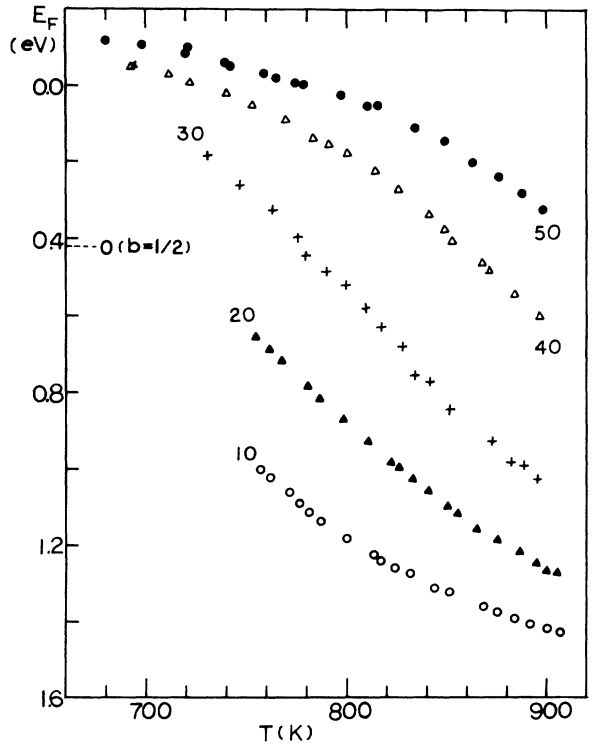

FIG. 10. Dependence of E_F on T for $x=10$–50. The reference energy is the top of the linear band, and the zero of the joined parabolic band at 0.42 eV is indicated.

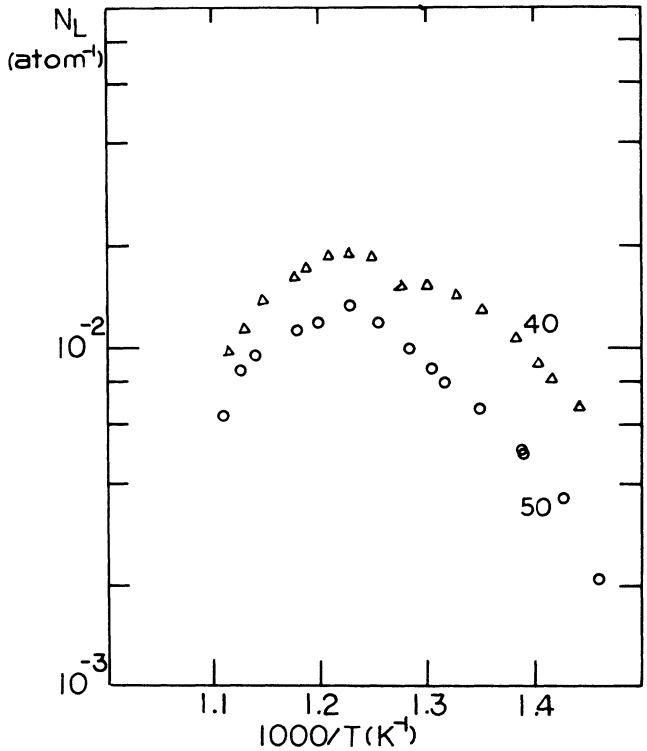

FIG. 11. Density of spin states in the acceptor band vs temperature for $x=40$ and 50. This is normalized to the density of atoms (2.7×10^{22} cm^{-3}).

It is possible to combine the curves for $N(E_F)$ for the parabolic and linear regions to provide the basis of a rigid band model for $N(E)$ in which E_F changes continuously as a function of T and x. When this is done, it is found that in the region where the acceptor band is merging with the valence band, there is a rapid increase in n and E_F which is responsible for the apparent increase in the activation energy of σ (1.3 eV). This behavior of σ has long been a puzzle.[2] It characterizes a region (II) in the x-T diagram separating the metallic region (III) where the temperature derivative of σ rapidly decreases from the semiconductor region (I) where the Maxwell-Boltzmann approximation is valid and the activation energy of σ (0.8 eV) agrees with that of S. When the explanation in terms of the absorption of acceptor states into the valence band was originally proposed, there were difficulties in the model. These were due in part to the fact that the concept of positive D^+ bond defects had not yet been discovered. The existence of positively charged centers other than holes has made it possible to understand the behavior of E_F. The present work seems to have yielded a reasonable detailed explanation for region II in terms of this model.

The validity of the rigid band model requires further comment. The mathematical character of the theoretical relations used in this work results in information about $N(E)$ which is valid within a distance $\approx kT$ from E_F in the metallic region, and the same distance from the mobility edge in the semiconductor region. There is no assurance that $N(E)$ remains the same when E has a larger separation from E_F. What we find is that $N(E)$ in the vicinity of E_F is nearly invariant when E_F has the same values with different combinations of x and T. But the accessible range of values of x for a given value of E_F is fairly limited (see Fig. 10), and all we can say is that the band behaves as if it is rigid near E_F over that limited composition range. The rigid band model is a convenient device in thinking about the band structure in this alloy system, but it is not likely to be valid over large changes in composition.

Finally, we wish to comment on the implications of our results for the use of microscopic heterogeneous models for the semiconductor-to-metal transition in liquid Se-Te alloys. As mentioned in the Introduction, there is a close correlation between the electronic transition which we have analyzed here and anomalies in the thermodynamic properties.[3] This is exemplified by quantitatively similar curves relating the transition temperature to the composition. We show the values of the thermodynamic transition temperature T_t in Table I. The thermodynamic behavior suggests that a change in the atomic arrangement may be taking place, but it differs from a phase transition in that the change is spread over a wide temperature range ($\approx 200\,^\circ$C). Several authors have proposed models based on the existence of microscopic clusters of two phases, one metallic and the other a semiconductor.[14–16] They have used formulas based on microscopic heterogeneity to describe the electronic behavior, and relate this to the thermodynamic behavior in terms of a parameter C which describes the relative amounts of the two phases. To be valid for the description of electronic transport, these clusters must have a minimum size of about 30 atoms. Our work has shown that the electronic behavior can be quite adequately described in terms of conventional concepts for a homogeneous system. Many of the "two-phase" equations which have been used, particularly for the thermodynamic parameters, are nearly equally valid when applied to a homogeneous mixture of two constituents. Therefore, successful explanation of some of the behavior by their use should not be taken as evidence for the existence of microscopic heterogeneity.

ACKNOWLEDGMENT

This work was supported by a National Science Foundation Grant No. DMR-8320547.

[1] J. C. Perron, Adv. Phys. **16**, 657 (1967).
[2] M. Cutler, *Liquid Semiconductors* (Academic, New York, 1977).
[3] M. Cutler and H. Rasolondramanitra, in *Localization and Metal-Insulator Transitions,* edited by H. Fritzsche and D. Alder (Plenum, New York, 1985), p. 199.
[4] R. Fainchtein and J. C. Thompson, Phys. Rev. B **27**, 5967 (1983).
[5] H. Thurn and J. Ruska, J. Non-Cryst. Solids **22**, 331 (1976).
[6] K. Takimoto and H. Endo, Phys. Chem. Liq. **12**, 141 (1982).
[7] S. Takeda, H. Okazaki, and S. Tamaki, Phys. Rev. B **31**, 7452 (1985).
[8] J. A. Gardner and M. Cutler, Phys. Rev. B **14**, 4488 (1976).
[9] M. Cutler, *Liquid Semiconductors,* Ref. 2, Chap. 4; H. Rasolondramanitra and M. Cutler, Rev. Sci. Instrum. **55**, 602 (1984).
[10] M. Cutler and H. Rasolondramanitra, J. Non-Cryst. Solids **61-62**, 1094 (1984).
[11] M. Cutler, *Liquid Semiconductors,* Ref. 2, Chap. 6.
[12] M. Cutler, *Liquid Semiconductors,* Ref. 2, Appendix B.
[13] This procedure contains a somewhat arbitrary element arising from positioning the theoretical curve to overlap the experimental one in Fig. 8 at the highest T. Lower positions would be equally valid, which would cause the calculated acceptor band spin density in Fig. 11 to be larger at high T.
[14] R. J. Hodgkinson, Philos. Mag. **23**, 673 (1971).
[15] M. H. Cohen and J. Jortner, J. Phys. (Paris) Colloq. **35**, C4-345 (1974).
[16] Y. Tsuchiya and E. F. W. Seymour, J. Phys. C **15**, L687 (1982).